POLITECNICO DI TORINO
Repository ISTITUZIONALE

Design and Realization of a Low Cross-Polarization Conical Horn with Thin Metasurface Walls

Original
Design and Realization of a Low Cross-Polarization Conical Horn with Thin Metasurface Walls / Sozio, V.; Martini, E.; Caminita, F.; De Vita, P.; Faenzi, M.; Giacomini, A.; Sabbadini, M.; Maci, S.; Vecchi, G.. - In: IEEE TRANSACTIONS ON ANTENNAS AND PROPAGATION. - ISSN 0018-926X. - 68:5(2020), pp. 3477-3486. [10.1109/TAP.2020.2975253]

Availability:
This version is available at: 11583/2799218 since: 2020-02-29T21:08:21Z

Publisher:
IEEE

Published
DOI:10.1109/TAP.2020.2975253

Terms of use:

This article is made available under terms and conditions as specified in the corresponding bibliographic description in the repository

Publisher copyright
IEEE postprint/Author's Accepted Manuscript

©2020 IEEE. Personal use of this material is permitted. Permission from IEEE must be obtained for all other uses, in any current or future media, including reprinting/republishing this material for advertising or promotional purposes, creating new collecting works, for resale or lists, or reuse of any copyrighted component of this work in other works.

(Article begins on next page)

12 October 2024

Design and Realization of a Low Cross-Polarization Conical Horn with Thin Metasurface Walls

V. Sozio, E. Martini, *Senior Member, IEEE*, F. Caminita, P. De Vita, M. Faenzi, A. Giacomini, *Member, IEEE*, M. Sabbadini, S. Maci, *Fellow IEEE*, G. Vecchi, *Fellow IEEE*

***Abstract*—A Ku-band low cross-polarization conical horn based on thin metasurface walls is presented in this paper, along with the relevant design method. The necessary boundary conditions are realized by printing a tensor metasurface on the internal walls of the horn, which yields a radiation performance similar to a standard corrugated Gaussian horn, yet with the benefits of thin walls. The design method is based on the adiabatic approximate solution for the hybrid mode of a conical waveguide with generic balanced impedance walls, which allows the determination of the impedance profile supporting a single balanced mode. The impedance design is based on the usual locally flat approximation of the wall and on the assumption of plane wave incidence. This approach results in an analytic design method that requires no optimization. The design has been first validated by solving the problem with homogenized impedance boundary conditions through a Body of Revolution (BoR) method of moments. The actual structure, including impedance wall implementation, is then simulated in full detail with a full-wave fast code. Finally, the horn has been realized and experimentally characterized; measurements show excellent agreement both with theory and with simulations, with cross-polarization level below -20dB over a two GHz bandwidth.**

***Index Terms*—Horn antennas, hybrid modes, metasurfaces, modal analysis, surface impedance.**

I. Introduction

HORN antennas with symmetric radiation properties and low cross-polarization for an efficient illumination of reflector antennas have been under investigation since the 1960s. Smooth wall circular horns can be designed by combining two modes [1], achieving axial symmetry and low cross-polarization in the radiation pattern, but limited bandwidth as a drawback. The advent of corrugated horns [2], [3] has overcome the narrow band issue, still maintaining axial beam symmetry, low side lobes, and low cross-polarization, thus, representing a milestone in the history of horn feeds [4].

In [3], it is demonstrated that symmetric patterns can be obtained with HE-EH hybrid modes. Anisotropic Impedance Boundary Conditions (AIBCs) at the horn walls are required to support these hybrid modes. In particular, surface impedances must satisfy the so called "balanced" hybrid condition to ensure low (theoretically zero) cross-polarization. An "artificial" surface is therefore needed to achieve this condition [5]. Corrugations, both transverse to the direction of the wave and longitudinal (with dielectric filling material), are the most known and largely used implementations of these artificial surfaces. Referring to the boundary conditions in acoustic, transversely and longitudinally corrugated surfaces have been described as artificial soft and hard surfaces, respectively [6]. In [7] these concepts are applied to the design of hybrid-mode horn antennas.

Soft and hard AIBCs are special cases of the balanced hybrid condition: soft horns assure low sidelobes, but low gain; hard horns have high gain but also high sidelobe level; a compromise with a good gain and an acceptable sidelobe level can be achieved by using finite wall impedances that respect the balanced hybrid condition. Soft hybrid mode horns have been designed with foam or solid dielectric cores (one or two) and strip loaded walls; hard hybrid mode horns have been realized with strip loaded walls with and without vias, or with two dielectric cores (see [8] for a complete review about soft and hard horn antennas).

The development of dual dielectric-core horn antennas capable of being designed to satisfy any (balanced) AIBCs between the soft and hard one first appears in [9], [10]. However, dielectric loaded horns are characterized by heavy weight and high losses.

The advent of Metamaterials (MTMs) and Metasurfaces (MTSs) and their increasing comprehension has inspired the realization of synthetic surfaces for symmetric pattern horn antennas [11]. An approach based on metasurfing [12] has been used to address sectoral H-plane horns [13]. In [14],

This work was supported by the Italian Space Agency (ASI) and the European Space Agency (ESA) under Contract No. 4000113142/15/NL/IA.
V. Sozio was with Links Foundation, Via Pier Carlo Boggio, 61, 10138 Torino, Italia (e-mail: valentina.sozio@virgilio.it).
E. Martini, M. Faenzi and S. Maci are with the Department of Information Engineering and Mathematics, University of Siena, Siena, Italy (e-mail: martini@dii.unisi.it, faenzi@diism.unisi.it, macis@dii.unisi.it).
F. Caminita is with Wave Up Srl, 53100 Siena, Italy (e-mail: francesco.caminita@wave-up.it).
P. De Vita is with Ingegneria dei Sistemi (IDS), 56121 Pisa, Italy (e-mail: p.devita@idscorporation.com).
A. Giacomini is with Microwave Vision Italy s.r.l., 00071, Pomezia, Italy (e-mail: andrea.giacomini@mvg-world.com).
M. Sabbadini was with Antenna & Sub-Millimetre Waves Section, Radio Frequency Payloads & Technology Division, ESA – ESTEC, NL-2200 AG Noordwijk, The Netherlands (e-mail: marco.sabbadini@ziggo.nl)
G. Vecchi is with the Department of Electronics and Telecommunications, Politecnico di Torino, 10144 Torino, Italy (e-mail:giuseppe.vecchi@polito.it).

hybrid-mode soft and hard horn antennas are designed for the first time with an ideal low index metamaterial wall, as an attractive alternative to the dual dielectric-core horns. In [15], metasurface walls, implemented with metallic FSS type screens and vias on a grounded dielectric layer, are engineered with a genetic algorithm optimization to provide soft, hard and balanced hybrid conditions in conical horn antennas over a wide bandwidth. The design is corroborated by full-wave simulations. In [16], MTS impedance tapering is introduced to improve radiation characteristics and impedance matching over a broader bandwidth; also in this case, the design is verified through simulations. The impedance tapering profile in [16] is determined through an optimization procedure based on the full-wave analysis of the whole horn structure. However, this kind of optimization can be very time consuming. On the other hand, a design approach based on a quasi-analytical modal analysis (similar to what is done for corrugated horns) has the advantage to be computationally inexpensive, while providing a physical insight into the horn behavior.

In this paper, a modal field-based method [7], [17], [18], [19] is applied for the design of low cross-polarization conical horns with engineered MTSs walls. As it is well known, the definition of modes in a structure requires the separability of the wave equation and of the BCs in the appropriate coordinate system. In a conical waveguide with impedance walls, separability is possible only for PEC/PMC BCs and, approximately, for soft/hard cases. The latter are important, since they model conical corrugated horns [4], [17], [18].

The conical mode analysis has also been extended in the adiabatic approximation to conical horns with arbitrary wall impedances [7]. This will be our starting point to develop an analytical-based design method for this class of horns.

The paper is structured as follows. Section II presents the conical adiabatic mode solution for impedance walls, and its use on a truncated conical horn. A numerical validation supporting the theoretical considerations is presented through a body of revolution Method of Moments (MoM) analysis with the use of realistic homogenized boundary conditions. Section III presents the low cross-polarization metahorn design, including implementation of the theoretical AIBC through subwavelength slotted patches, and numerical full-wave results of the detailed antenna structure. Section IV presents manufacturing and measurements of the antenna. Finally, conclusions are drawn in Section V.

II. Conical Modes for Impedance Walls

A metahorn is a metallic horn antenna whose interior walls are coated with a dielectric material printed with a metallic texture consisting of subwavelength patches, as shown in Fig. 1. A spherical coordinate system (r,θ,ϕ) is introduced as depicted there, where r is the radial distance from the cone vertex. We denote with a and w_g the largest and the smallest circular sections of the horn, respectively, and with θ_1 the half flare angle.

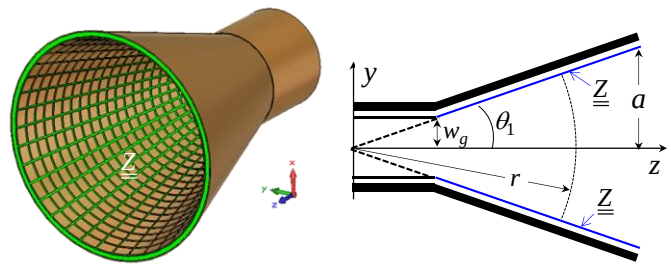

Fig. 1. Pictorial representation of the metasurface horn, and geometry of its longitudinal cross-section.

The MTS is effectively modelled in terms of an equivalent anisotropic impenetrable IBC [20], characterized by a diagonal tensor, whose matrix representation in spherical coordinates is

$$\underline{\underline{Z}} = \begin{bmatrix} Z_r & 0 \\ 0 & Z_\phi \end{bmatrix} \tag{1}$$

All the entries are purely reactive in the absence of losses, as implied in the following.

A. Characteristic Equation

Separation of variables, as described in [7], [17], [18], yields the characteristic equation for the conical modes [19]. As a consequence of the periodicity condition dictated by the rotational symmetry of the horn structure, the azimuthal index must be an integer number. We denote this number by m. For any m, a non-integer radial index ν depends on the flare angle θ_1 and on the impedance entries via the following characteristic equation

$$\begin{aligned} &\left(p_\nu^m(\theta_1) - \frac{\nu(\nu+1)}{jkr\eta_0} Z_\phi \right) \cdot \\ &\left(p_\nu^m(\theta_1) - \frac{\nu(\nu+1)\eta_0}{jkr} (Z_r)^{-1} \right) = -\left(\frac{m h_\nu(kr)}{\sin\theta_1} \right)^2 \end{aligned} \tag{2}$$

where η_0 and k denote the free-space characteristic impedance and wavenumber, respectively, and $h_\nu(x) = \left[d\hat{H}_\nu^{(2)}(x)/dx \right] / \hat{H}_\nu^{(2)}(x)$, where $\hat{H}_\nu^{(2)}(x)$ is the Schelkunoff Hankel function of second kind and order ν. In (2), $p_\nu^m(\theta) = \left[dP_\nu^m(\cos\theta)/d\theta \right] / P_\nu^m(\cos\theta)$, where $P_\nu^m(\cos\theta)$ is the associated Legendre function of order m and degree ν. We note that the computation of the associated Legendre function requires the use of hypergeometric functions [21], [22].

B. Adiabatic Solution

A generic modal function solution of (2) is of the kind $F_{m\nu}(r,\theta_1)$. In this context, the presence of the radial coordinate r in the characteristic equation is a well-known problem, since it does not allow for an exact solution in the general case. This problem can be circumvented by resorting

to the so-called "adiabatic" approximation[2], which consists in considering the radial index to be a function of the radial position r via the solution of (2), *i.e.* $\nu = \nu(kr)$.

It is of interest to study the case $kR >> \nu$, for which the radial function simplifies to its asymptotic *constant* expression $h_\nu(kR) \approx -j$. In this case, it is apparent from (2) that the solution for ν is independent from the position r only if the impedance profile is of the kind

$$Z_\varphi(r) = j\frac{\eta_0 r}{C}; \quad Z_r(r) = -j\frac{\eta_0 C}{r} \tag{3}$$

where C is an arbitrary real constant. It is worth noting that in this case

$$Z_\varphi(r) \cdot Z_r(r) = \eta_0^{\,2} \tag{4}$$

which is the well-known balanced condition that ensures zero cross polarization [25], [3]. We note that this condition is also the same obtained in [15], [16] for conical balanced horns and in [26] for dual polarization mode in MTS antennas. Since in absence of losses the impedance entries are purely imaginary, (3) implies an opposite capacitive or inductive nature of the two impedances, together with a specific opposite dependence on r. This dependence is the first key point in our method. In fact, for $kr >> \nu$, the condition (3) leads to the following simple asymptotic form of the characteristic equation

$$\left(p_\nu^m(\theta_1) - \frac{\nu(\nu+1)}{Ck}\right)^2 = \left(\frac{m}{\sin\theta_1}\right)^2 \qquad kr >> \nu \tag{5}$$

the solution of which is independent of r, as occurs for conical modes in presence of PEC walls. It is therefore expected that the solution of the characteristic equation (2) under the balanced condition (3) is weakly dependent on r, becoming asymptotically constant for kr large. This is indeed observed in Fig. 2, where the solution of (2) for m=1 (dominant mode) is plotted as a function of r/λ for various flare angles. For increasing flare angles ν reaches its asymptotic value more rapidly. It is also worth noting that very close to the horn vertex (origin of the reference system) a very small imaginary part of ν is found for small flare angle, not depicted in Fig.2.

C. Local Incidence Angle

The smooth radial dependence of the radial index legitimates the mentioned local adiabatic solution $\nu(kr)$ obtained solving the characteristic equation of the conical section by section, and the use of it as a basic input for the MTS design. In doing that, it is important to account for the space-dispersivity of the homogenized MTS impedance in its practical realization with printed texture.

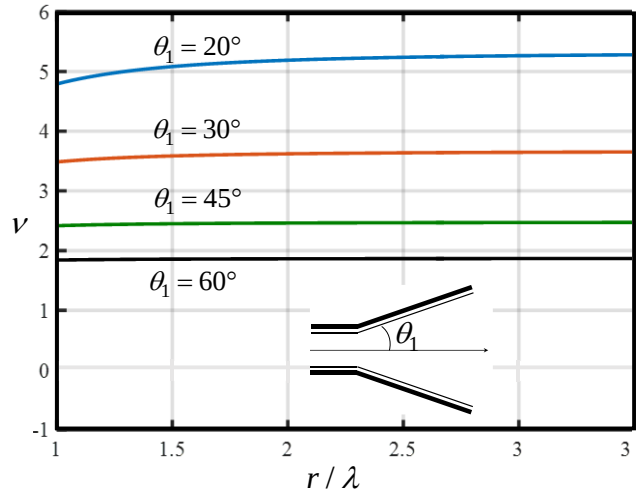

Fig. 2 Solution of (2) obtained with the use of (3) for various values of the flare angle and for C=0.06.

To this end, we assume that the local modal incidence angle is

$$\theta_{inc} = \arcsin\left\{\Re\mathrm{e}\left(\frac{k_r(r)}{k}\right)\right\} \tag{6}$$

where $k_r(r)$ is the normalized radial wavenumber of the mode, namely [4], [17]:

$$\frac{k_r(r)}{k} = jh_\nu(kr) = j\frac{\frac{\partial}{\partial kr}\hat{H}_\nu^{(2)}(kr)}{\hat{H}_\nu^{(2)}(kr)} = j\frac{\partial[\ln \hat{H}_\nu^{(2)}(kr)]}{\partial kr} \tag{7}$$

An example of the dependence of incidence angle on the radial position is shown in Fig. 3.

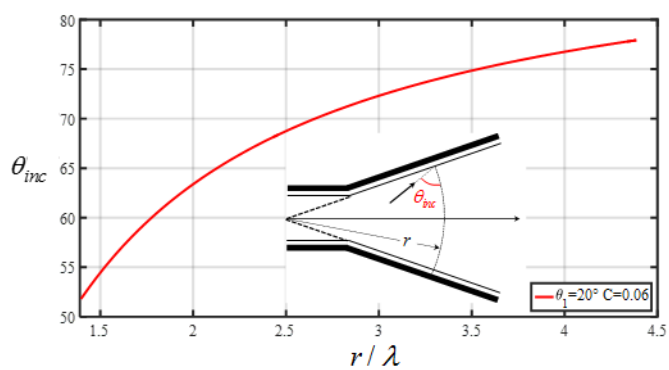

Fig. 3. Incidence angle as a function of the normalized radial position for a flare angle of the horn equal to 20° and C=0.06, under balanced hybrid condition (3).

D. Impenetrable vs Penetrable Impedance

The knowledge of the incidence angle, together with (3), is the second key point for the MTS synthesis. It is indeed well known [20], [27] that a MTS realized by printed elements over a grounded slab can be modelled by an "impenetrable" surface impedance, but the resulting value is dependent on the local

[2] In [23], [24] a modal field-based approach, based on the definition of "adiabatic modes", and their extension to "intrinsic modes", was presented as solution to propagation problems when separability conditions are not completely matched along the z axes. The work presented in those references was relevant to cylindrical structures which exhibit a local longitudinal variation of boundary conditions. Along a similar guideline, we use here an "adiabatic concept" to study the exact characterictic equation for conical boundaries.

wave-vector. This is because the homogenized impedance takes into account both the contribution of the grounded dielectric slab, typically wavevector dependent (and therefore requiring the knowledge of the local incidence angle, identified by (6) in our method), and of a homogenized "penetrable" impedance associated with the printed metallization. The latter is almost independent from the wave-vector in a broad frequency range. The resulting combination of the two contributions, approximated through a local transmission line model, leads to the impenetrable impedance.

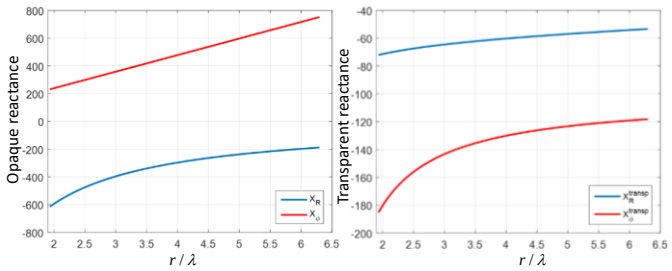

(a) (b)

Fig. 4. Impenetrable reactances (a) and penetrable reactances (b) vs. the radial distance from the horn vertex. Note the different ranges in the vertical scale.

Example of opaque (impenetrable) reactances X_ϕ, X_r and of transparent (penetrable) reactances X_ϕ^{transp}, X_R^{transp} are plotted in Fig.4 as a function of the radial normalized distance. The dielectric substrate selected for the MTS metallic printing has a thickness $h_d = 1.016\,mm$ and a permittivity of $\varepsilon_r = 3.6$. The example is relevant to a conical horn working at 12GHz with a flare angle 18.445°. The surface impedances are defined through (3) with C=0.0788 in order to obtain feasible values of the transparent impedance along the entire horn.

It is noted that the use of thinner substrates is also possible in principle, but it would require the use of patches with higher capacitance, which, in turn, would imply a narrower bandwidth for the metahorn.

E. Radiation patterns for truncated mode

It is interesting to investigate the radiated field obtained by truncating the conical unimodal horn. To this end, the equivalence principle is applied to a spherical cap passing from the rim of the truncated cone (see Fig. 5b) [17].

To validate the solution obtained with the modal adiabatic currents, a full wave MoM-BoR analysis method with penetrable impedance BCs has been applied to the analysis of the same structure [28]. In the MoM-BoR fomulation, the field of the TE11 mode at the horn throat is used as excitation, while the MTS is represented with a homogenized transparent impedance tensor over a grounded slab with $\varepsilon_r = 3.4$ (see Fig. 5d). The agreement between the two methods reveals the accuracy of the adiabatic mode model and the capability of the MTS to filter out spurious component deriving from the TE11 excitation. In particular, full wave simulations confirm that the chosen impedance profile is able to provide a very low cross-polar horn. Note that the adiabatic modal currents on the spherical cap rigorously predict zero cross polar components.

III. METAHORN DESIGN WITH HE_{11} MODAL REACTANCE

A. Impedance design with metallic patterning

The transparent impedance walls are next implemented in practice through the design of subwavelength cross-slotted patches printed on the grounded dielectric slab. Examples of the implemented unit cells are represented in Fig.6. The two arms of the cross slots etched inside the metal of the patches may have different lengths in order to manage with a certain independency the TE and TM components of the MTS tensor.

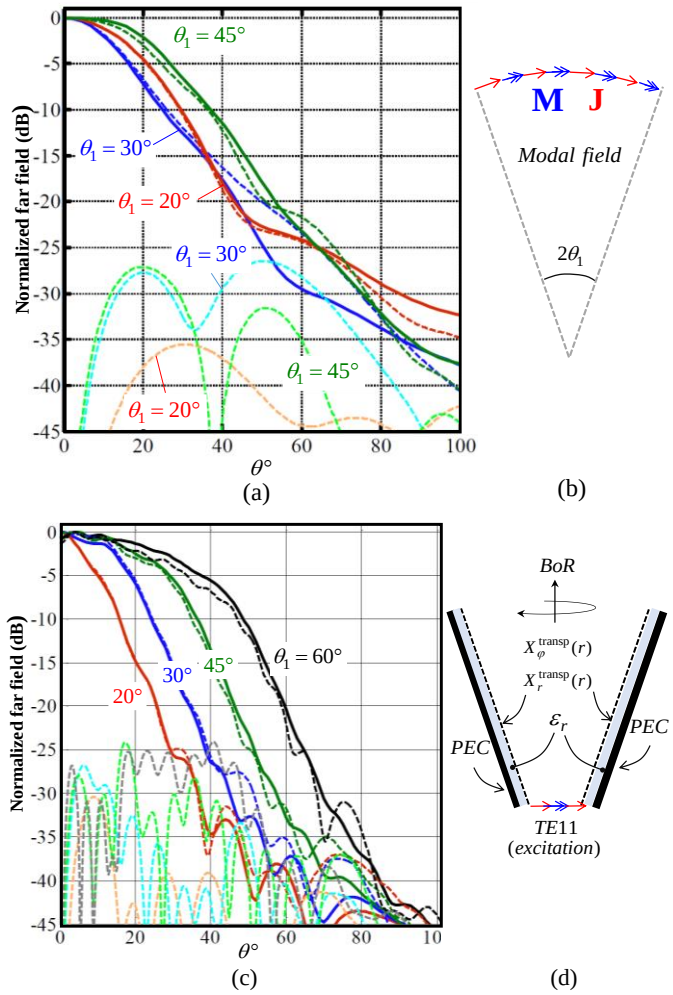

Fig. 5: Normalized far field radiation patterns as a function of the observation angle θ; comparison of two methods for various flare angles. (a) r_{max}=3λ ; (c) r_{max}=10λ (results obtained at 15 GHz). Solid lines: results obtained with equivalent modal currents over the aperture-cap radiating in free space (b); dashed lines: MoM–BoR results obtained with homogenized transparent reactance sheet impedance over grounded dielectric slab (d). Ecxcitation is provided by using field of a TE11 in circular waveguide.

It is worth noting that being the desired impedance only dependent on r, the cell geometries differ along the radial horn profile, while they do not change in the azimuthal direction.

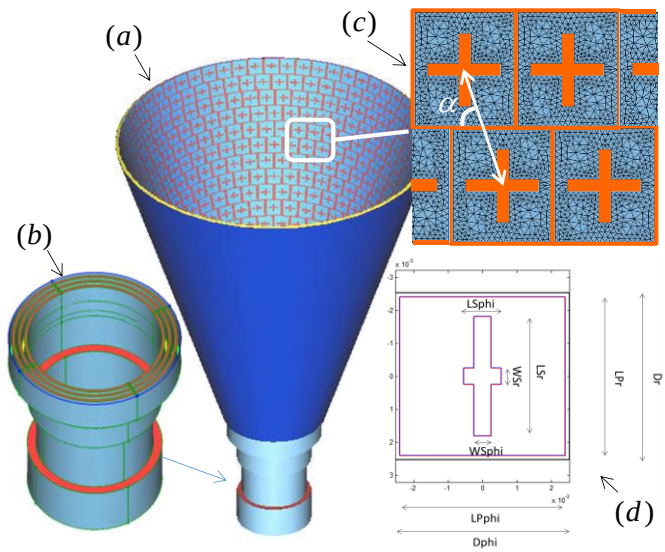

Fig. 6. (a) Numerical model of the horn with MTS constituted by metallic subwavelength patches with etched cross slots; (b) circular waveguide transition with longitudinal corrugations; (c) local planar periodic problem with triangular lattice and mesh; (d) geometric parameters of the individual cell for the surface impedance database construction by periodic MoM.

The identification of the unit cell geometry needed to get the desired transparent impedance is based on two assumptions: *i*) a local planar periodicity with a triangular lattice *ii*) a planar unit cell and a square patch contour. The assumption (*i*) means that in each individual position a patch is surrounded by identical patches, periodically distributed on a triangular (skew) lattice. This allows for the use of a MoM based on periodic boundary conditions. Concerning the assumption (*ii*), it consists in approximating the curved surface on which each patch is printed with a planar one, and the slightly trapezoidal shape of each patch with a square shape. This is done by a geometrical projection over the tangent plane in each point.

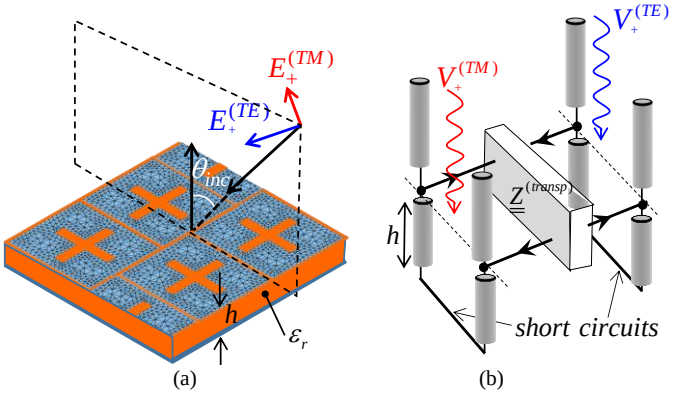

Fig. 7. (a) Local plane-wave incidence with modal incidence angle over the local flat MTS: (b) transmission line equivalent network for the retrieval of the anisotropic modal impedance.

The skewness of the lattice in (*i*) (Fig 6c) is fundamental for the accuracy of the impedance extraction. Indeed, accommodating an integer number of patches over azimuthal rings implies a different number of patches in radially contiguous rings; in turn, this implies a small misalignment between neighboring patches that can be adapted to a local periodicity only with a skew angle of the local lattice.

The geometry of the unit cell is depicted in Fig. 6. The period along the radial direction *Dr* is kept constant and equal to 5.2 mm (~λ/5); the period along the azimuthal direction *Dphi* is slightly varied around this value so as to accommodate an integer number of unit cells in each ring, ranging from 5.13mm to 5.33mm. From the theoretical model, each ring is characterized by an objective impedance and an incidence angle of the plane wave. Furthermore, the skewness angle of the lattice is determined by the unit cell period. In order to determine the right geometry of a local patch providing the desired value of impedance, a database has been constructed by analyzing unit cells with different geometries with a periodic MoM. The geometrical parameters involved in the database construction are the two lengths of the arms of the cross slot (*LSphi* and *LSr*), the skewness angle of the lattice. The size of the patches, *LPphi* and *LPr* varies slightly in each ring (*LPphi* ranges from 4 mm to 4.4 mm, *LPr* from 4.8 mm to 4.9 mm); the slot widths are kept constant and are equal to *WSphi*=*WSr*=0.51mm.

A relationship among the parameters and the values of the opaque impedances entries is established. The transparent reactance X_r, X_ϕ are individuated through a TE-TM two-port transmission line model, excited by a plane wave coming from the incidence modal angle (Fig. 7). The transmission line model is limited to the dominant Floquet-wave mode of the local periodicity, while the higher order modes are incorporated in the equivalent transparent reactance. The database is first constructed with a coarse sampling of the parameters values, and next interpolated to get continuous values. The research of the optimal set of geometrical parameters that realizes a given couple of reactance entries is done by an optimization algorithm. The research of the optimal value is facilitated by using the geometry of contiguous patches as an entry guess. We note that the required transparent impedance matrix is diagonal; since, in general, the skewed lattice may create a small coupling among the polarizations; this coupling must be compensated by acting on the degrees of freedom of the unit cell.

B. Launcher

In order to emulate the hybrid port of the conical horn, a mode-launching region of the horn must be designed to transform a TE_{11} mode in input circular waveguide into a hybrid HE_{11} mode at its output section (horn throat). The longitudinal profile of the final structure is reported in Fig. 8. The optimized values of the geometrical parameters are reported in TABLE I.

TABLE I
GEOMETRICAL PARAMETERS OF THE LAUNCHING SECTION

wg_{in}	wg	d_1	r_1	r_2	r_3	r_4
11.9 mm	15.24 mm	10.37 mm	12.4 mm	13 mm	13.5 mm	14.10 mm
r_5	$hcwg_1$	$hcwg_2$	$hcwg_3$	h_1	h_2	h_3
14.6 mm	10 mm	12.6 mm	15.96 mm	3.85 mm	7.95 mm	6.49 mm

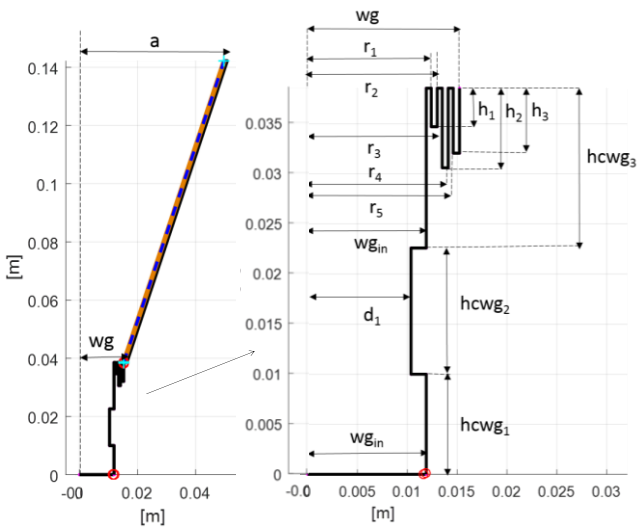

(a) (b)

Fig. 8. Longitudinal profile of the horn with semi-flare angle 18.445°, a=49.8mm, wg=15,24mm (a) and of the launcher section (b). The valued of the parameters for the launching section are reported in Table I.

C. *Full-wave MLFMM analysis*

The final design in Fig. 8 has been analyzed by two software codes: a code by IDS based on a Multilevel Fast Multiple method (MLFMM) [29] and the aforementioned BoR-MoM code based on homogenized transparent impedance (see Fig. 5d). The results shown in Fig. 9 present a final comparison among the results obtained by the MLFMM, the BoR-MoM and the modal currents over the aperture-cap radiating in free space (like in Fig. 5b). The MLFMM results are obtained by exciting the circular waveguide cross-section with a horizontal dipole; while the results from BoR-MoM have been obtained by exciting the circular waveguide section with a TE_{11} mode. Surprisingly, it is seen that the results by the modal aperture currents predict accurate co-polar pattern up to -10dB from the maximum. The accuracy of the BoR-MoM analysis is also surprising, since the analysis is based on homogenized theoretical values of the impedance surface.

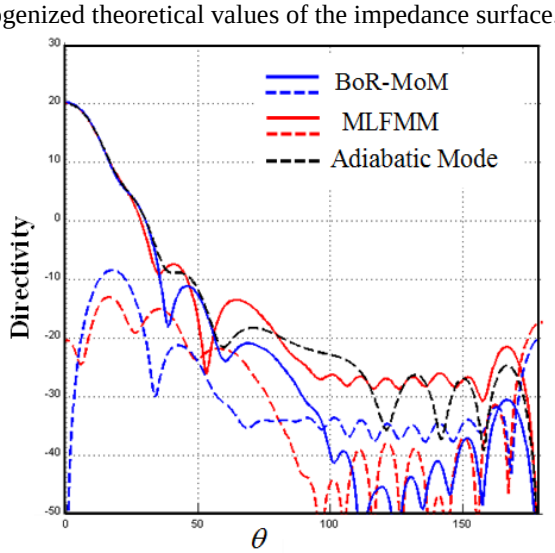

Fig. 9. Comparisons of the radiation patterns obtained from various numerical models for the final geometry in Fig. 8.

Fig. 10. Final Metahorn Engineering Model.

IV. Manufacturing and Measurements

A. *Manufacturing*

The realized conical metahorn is shown in Fig. 10. It has been realized by using a flexible substrate on which the metasurface is printed. An intermediate rigid dielectric substrate machined to conical shaped is placed between the metasurface and the metallic wall. The outer conical horn is made of aluminum alloy and it is manufactured by means of traditional CNC turning machine. Several materials have been traded-off for the intermediate conical slab. The most appropriate resulted to be ULTEM™ 2300 [30], an amorphous thermoplastic polymer which combines mechanical, thermal and electrical properties. According to measurements conducted with a WR75 waveguide set-up on two material samples, dielectric relative permittivity is 3.62 at X-band, loss tangent varies between 0.029 and 0.050 in the frequency range 10-15GHz. This has been bonded onto the inner wall of the metallic horn. The flexible substrate is DuPont™ Pyralux AP8545R [31]. This material is a copper-clad laminate based on a polyimide film bonded to copper foil. Among its main characteristics, this material is flexible, highly reliable and temperature resistant. The thickness chosen for the substrate is 4 mils (100 microns), the relative dielectric constant is 3.3 at X-band, the loss tangent is 0.004.

The substrate has been printed in plane by a photolithographic process, curved and bonded over the rigid dielectric part in autoclave with the help of a conical mold. The total thickness of the dielectric slab and the flexible printed circuit board matches the nominal design value of 1mm. The transition between the circular waveguide and the conical horn is done by CNC turning machine and fastened to the conical part with a precision flange. The metallic launcher is composed by several axial corrugations (see Fig. 8). A commercial Ortho-Mode Transducer (OMT) is connected to the corrugated launcher in order to feed the two linear polarizations (H/V) of the conical horn with high purity and port-to-port decoupling.

Fig. 11. Antenna under test in the MVG Star Lab 18 spherical near field antenna test range.

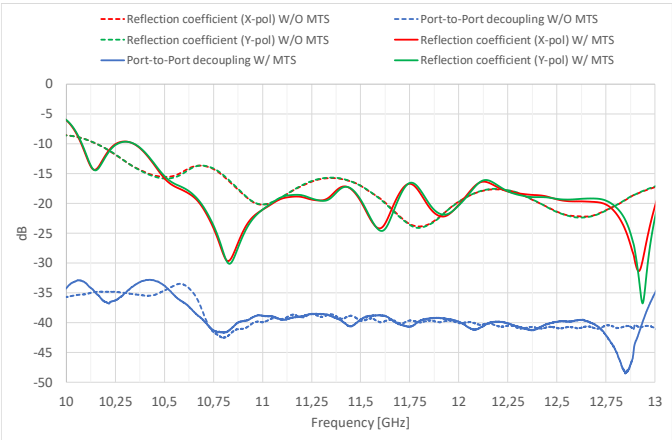

Fig. 12. Scattering parameters at the input ports of the bare metallic horn (dashed lines) and of the metahorn (continuous lines).

B. *Measurements*

Scattering parameters of the manufactured horn have been measured in a fully anechoic chamber at Microwave Vision Group (MVG) (Italy, Pomezia) using an Anritsu Vector Analyzer (MS4647B). The accuracy of the test set-up is +/-0.05 dB at -0.5dB levels and +/-1dB at -30dB levels. The radiation pattern has been measured with the MVG Star Lab 18 spherical near field antenna test range [32] (Fig. 11), equipped with 14 probes in the range 6-18 GHz, mounted with equal spacing on a circular arch. The geometry of the set-up ensures minimum interference and low ripple on the radiation patterns. The measured S-parameters at the input coaxial ports of the horn, including the OMT, are shown in Fig. 12. The resulting operational bandwidth, considering -15dB reflection coefficient, ranges from 10.5 to 13 GHz, with a port-to-port decoupling better than -35dB. These achieved results widely cover the expected frequency range. For the sake of comparison, the same figure also reports the reflection coefficient for the same conical horn without MTS, i.e. with bare metallic walls. As it can be seen, the presence of the MTS does not degrade the input port matching and the port-to-port decoupling.

Sample results of measured RHCP and LHCP radiation patterns are shown in Fig. 13 in the frequency range 10.7-12.5 GHz. These results are obtained by measuring the two linear polarizations of the horn independently and then computing the resulting circular polarization in post-processing, assuming ideal feeding with equal amplitude and phase quadrature between the coaxial ports. To minimize the impact of the OMT un-idealities on the measured axial ratio, its channel imbalance between ports is calibrated out.

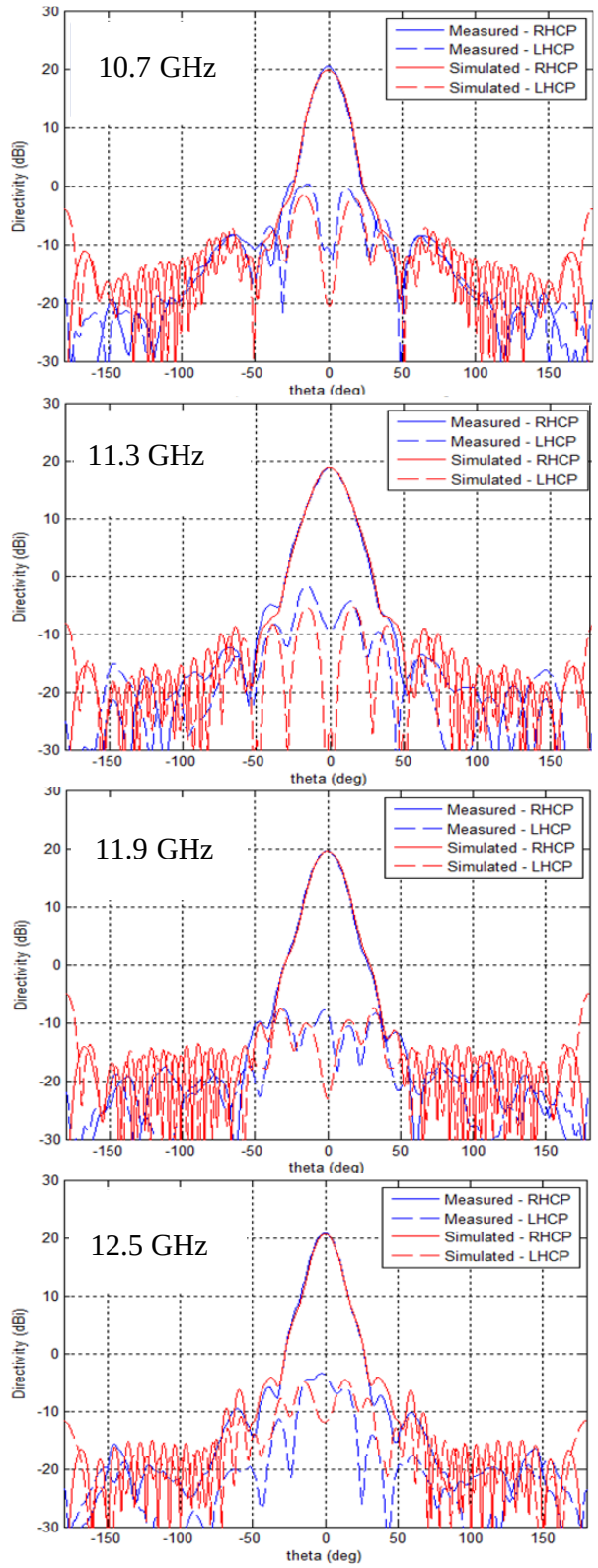

Fig. 13. Directivity patterns at various frequencies; comparison between measurements and simulation (MLFMM, IDS code)

The plots shown in Fig. 13 also present the numerical results calculated with MLFMM tool from IDS, showing a good agreement in a range of -30 dB level. The adiabatic mode simple prediction (not shown here for not overcrowding the pictures) actually shows an accuracy over -30 dB from the co-polar components, namely of the same order of those in Fig. 9. This confirms the validity of the extremely simplified method as an effective and reliable design tool for initial sizing of the structure. The overall performances in the operational bandwidth are illustrated in Figs. 14-17. In particular, Fig. 14 reports the maximum directivity, Fig. 15 the peak cross-polarization level with respect to the maximum co-polarized field, and Fig. 17 the radiation efficiency. In order to better highlight the improvement introduced by the MTS, the performance of the metallic horn without MTS are also reported in the same figures.

Cross-polar discrimination (XPD) has been calculated as the difference between the co-polar component at broadside and the maximum value of the cross-polar component in the main beam angular region $|\theta|<17°$. It is seen that between 11GHz and 13 GHz, the cross-polar level is 25dB below peak in average, with minima beyond 30dB. These levels are comparable with the achievable performance of a generic corrugated horn. The improvement with respect to the bare metallic horn is around 10dB.

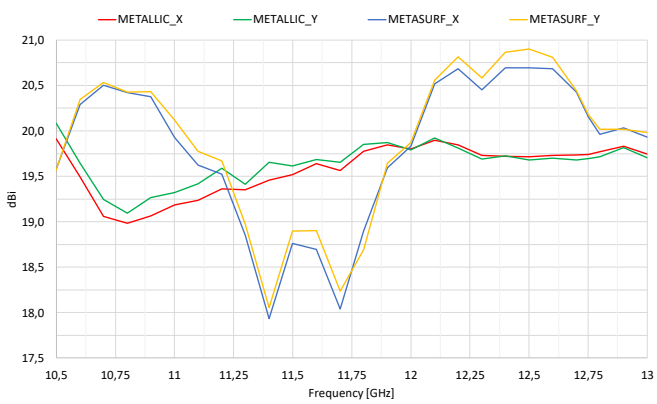

Fig. 14. Measured maximum directivity as a function of frequency for the proposed metahorn prototype and for the same horn without MTS.

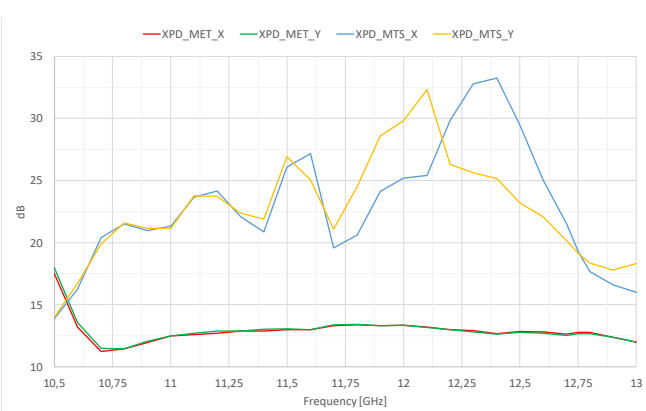

Fig. 15. Measured cross-polar discrimination as a function of frequency for the proposed metahorn prototype and for the same horn without MTS.

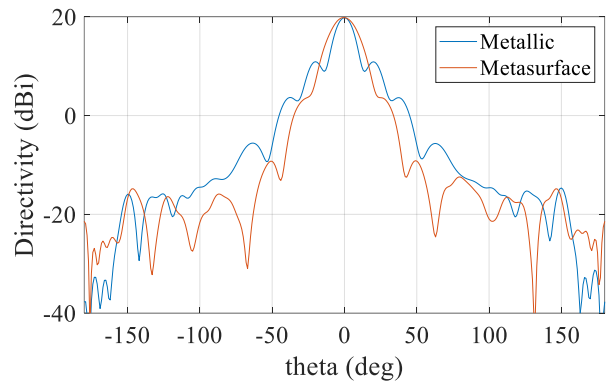

Fig. 16. Measured co-polar pattern in the E-plane at 12GHz for the proposed metahorn prototype and for the same horn without MTS.

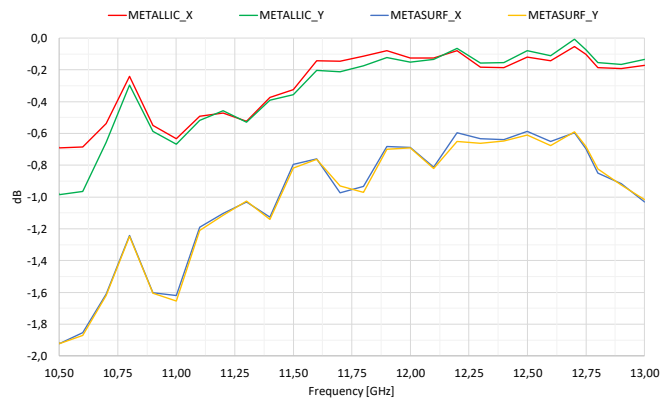

Fig. 17. Measured radiation efficiency as a function of frequency for the proposed metahorn prototype (blue and yellow lines) and for the same horn without MTS (red and green lines)).

On the other hand, the insertion of the MTS implies a slight decrease of the radiation efficiency (between 0.5dB and 1dB), mainly due to dielectric losses. This aspect could be improved by selecting materials with a lower loss tangent.

Finally, in order to show the improvement introduced by the MTS in the side lobe level, co-polar radiation patterns in the E-plane (X-polarization) are shown in Fig. 16 for both the metahorn and the bare metallic horn. As it can be seen, SLL is significantly improved in the presence of the MTS. A similar behavior is also found at the other frequencies of the operational band.

V. Conclusion

A low cross-polarization conical horn based on thin metasurface walls is presented. The design is performed by emulating with printed metasurfaces the boundary condition supporting the HE_{11} mode in conical waveguide with anisotropic impedance BCs on the walls. These BCs exhibit $1/r$ and r dependencies for the two components of the tensor impedance, and they support a mode perfectly balanced in polarization. The tensor-impedance is implemented by printing patches with two slots over a grounded slab, without using any optimization method for correcting the impedance. With respect to previously published solutions for metahorn implementation, the one proposed in this paper is simpler to manufacture since no vertical metalizations are required and it

offers the advantage of thinner walls and reduced mass with respect to a corrugated horn. These characteristics, combined with the possibility to shape the radiation pattern by redesigning the MTS, make the proposed design particularly suitable for space applications, where performance requirements are demanding, and mass and bulkiness reduction are of primary importance. Final measurements of a 20dB gain Ku-band prototype have evidenced a cross-polar level below -20 dB over 2GHz bandwidth around 12GHz, with a best performance of less than -30dB.

ACKNOWLEDGMENT

The work has been developed under ESA (ESA-ESTEC, Noordwijk, The Netherland) contract n. 4000113142/15/NL/IA, under agreement with the Italian Space Agency in the framework of the ARTES programme. The authors wish to thank the other participants to the project, in particular R. Ravanelli, Thales Alenia Space, Italy, A. Francavilla, Istituto Superiore Mario Boella, L. Foged, Microwave Vision Group, Italy, and the company GERG GmbH for manufacturing of the engineering model.

REFERENCES

[1] P. D. Potter, "A new horn antenna with suppressed sidelobes and equal beamwidth," *Microwave J*., Vol. 6, pp. 71–78, June 1963.

[2] J. Simmons and A. F. Kay, "The Scalar Feed—A High Performance Feed for Large Paraboloid Reflectors," *IEE Conf. Publ.* 21, pp. 213–217, 1966.

[3] H. C. Minnett and B. M. Thomas, "A Method of Synthesizing Radiation Patterns with Axial Symmetry," *IEEE Trans. Antennas Propagat*., vol. AP-14, pp. 654–656, Sept. 1966.

[4] P. J. B. Clarricoats and A. D. Olver, "Corrugated horns for microwave antennas," in *Inst. Elec. Eng. Electromagnetic Waves*, Series 18. London: Peregrinus, 1984, Ch. 3.

[5] V. H. Rumsey, "Horn Antennas with Uniform Power Patterns Around Their Axes," *IEEE Trans. Antennas Propagat*., vol. AP-14, pp. 656–658, Sept. 1966.

[6] P. S. Kildal, E. Lier and J. A. Aas, "Artificially soft and hard surfaces in electromagnetics and their application," *Antennas and Propagation Society International Symposium*, 1988. AP-S. Digest, Syracuse, NY, USA, 1988, pp. 832-835 vol.2.

[7] Erik Lier, Per-Simon Kildal, "Soft and Hard Horn Antennas", *IEEE Transactions on Antennas and Propagation*, vol. 36, no. 8, August 1988.

[8] Erik Lier., "Review of Soft and Hard Horn Antennas, Including Metamaterial-Based Hybrid-Mode Horns," *IEEE Antennas and Propagation Magazine*, Vol. 52, No. 2, April 2010.

[9] E. Lier, "Hybrid-Mode Horn Antenna with Design-Specific Aperture Distribution and Gain," *IEEE International Symposium on Antennas and Propagation*, Columbus, OH, June 22-27, 2003, pp. 502-505.

[10] E. Lier and A. Kishk, "A new class of dielectric-loaded hybrid-mode horn antennas with selective gain: design and analysis by single mode model and method of moments," in *IEEE Transactions on Antennas and Propagation*, vol. 53, no. 1, pp. 125-138, Jan. 2005.

[11] E. Lier, D. H. Werner and T. S. Bird, "The Evolution From Metal Horns to Metahorns: The development of EM horns from their inception to the present day," in *IEEE Antennas and Propagation Magazine*, vol. 61, no. 4, pp. 6-18, Aug. 2019.

[12] S. Maci, G. Minatti, M. Casaletti and M. Bosiljevac, "Metasurfing: Addressing Waves on Impenetrable Metasurfaces," in *IEEE Antennas and Wireless Propagation Letters*, vol. 10, no. , pp. 1499-1502, 2011.

[13] M. Bosiljevac, M. Casaletti, F. Caminita, Z. Sipus and S. Maci, "Non-Uniform Metasurface Luneburg Lens Antenna Design," in *IEEE Transactions on Antennas and Propagation*, vol. 60, no. 9, pp. 4065-4073, Sept. 2012.

[14] E. Lier and R. K. Shaw, "Design and simulation of metamaterial-based hybrid-mode horn antennas," *Electron. Lett*., vol. 44, pp. 1444-1445, 2008.

[15] Qi Wu, Clinton P. Scarborough, Douglas H. Werner, Erik Lier, and Xiande Wang, "Design Synthesis of Metasurfaces for Broadband Hybrid-Mode Horn Antennas With Enhanced Radiation Pattern and Polarization Characteristics," *IEEE Transactions On Antennas And Propagation*, Vol. 60, No. 8, August 2012.

[16] Qi Wu; Scarborough, C.P.; Werner, D.H.; Lier, E.; Shaw, R.K. "Inhomogeneous Metasurfaces With Engineered Dispersion for Broadband Hybrid-Mode Horn Antennas," *Antennas and Propagation, IEEE Transactions on*, On page(s): 4947 - 4956 Volume: 61, Issue: 10, Oct. 2013.

[17] P. J. Clarricoats and P. K. Saha, "Propagation and Radiation Behavior of Corrugated Feeds," *IEE Proc*., vol. 118, parts 1 and 2 (September 1971): 1167–1186.

[18] A. D. Olver and J. Xiang, "Wide angle corrugated horns analysed using spherical modal-matching," in *IEE Proceedings H - Microwaves, Antennas and Propagation*, vol. 135, no. 1, pp. 34-40, Feb. 1988.

[19] V. Sozio, M. Faenzi, M.A. Francavilla, E. Martini, F. Caminita, M. Sabbadini, S. Maci, G. Vecchi, "Low Cross Polarization Conical MetaHorn Based on an Adiabatic Mode Formulation", *11th European Conference on Antennas and Propagation (EuCAP)*, Paris, 19-24 March 2017

[20] E. Martini, M. Mencagli, S. Maci, "Metasurface transformation for surface wave control," *Philosophical Transactions of the Royal Society A: Mathematical, Physical and Engineering Sciences*, 373 (2049), art. no. 20140355, 2015.

[21] J. Pearson, "*Computation of hypergeometric functions*", thesis for the degree of Master of Science in Mathematical Modelling and Scientific Computing at the University of Oxford, September 2009.

[22] J. Pearson, Matlab routines for the computation of hypergeometric functions hosted in the website: http://people.maths.ox.ac.uk/porterm/research/hypergeometricpackage.zip

[23] J. M. Arnold and A. Dendane, "Intrinsic mode theory of conical corrugated horns," in *IEE Proceedings H - Microwaves, Antennas and Propagation*, vol. 136, no. 3, pp. 250-256, June 1989.

[24] L. B. Felsen and L. Sevgi, "Adiabatic and intrinsic modes for wave propagation in guiding environments with longitudinal and transverse variation: formulation and canonical test," in *IEEE Transactions on Antennas and Propagation*, vol. 39, no. 8, pp. 1130-1136, Aug 1991.

[25] A. D. Olver, P. J. B. Clarricoats, and L. Shafai, *Microwave Horns and Feeds*. London, U.K.: Inst. Electr. Eng., 1994.

[26] A. Tellechea Pereda et al., "Dual Circularly Polarized Broadside Beam Metasurface Antenna," in *IEEE Transactions on Antennas and Propagation*, vol. 64, no. 7, pp. 2944-2953, July 2016.

[27] M. Mencagli, E. Martini and S. Maci, "Transition Function for Closed-Form Representation of Metasurface Reactance," in *IEEE Transactions on Antennas and Propagation*, vol. 64, no. 1, pp. 136-145, Jan. 2016.

[28] F. Caminita, M. Faenzi, D. G. Ovejero and S. Maci, "Numerical issues in the analysis of large BoR antennas involving dielectric and metallic parts," *7th European Conference on Antennas and Propagation (EuCAP)*, Gothenburg, 2013, pp. 4043-4045.

[29] https://www.idscorporation.com/pf/galileo-suite/

[30] https://www.sabic.com/en

[31] https://www.dupont.com/content/dam/dupont/products-and-services/electronic-and-electrical-materials/flexible-rigid-flex-circuit-materials/documents/PyraluxAPclad_DataSheet.pdf

[32] https://www.mvg-world.com/en/system/files/starlab_2014.pdf